Iranian Journal of Materials Forming 10 (1) (2023) 26-38

Online ISSN: 2383-0042

IJMF

Iranian Journal of Materials Forming

Journal Homepage: http://ijmf.shirazu.ac.ir

Research Article

Comparison of Plastic Anisotropy and Crystallographic Texture Evolution of Aluminum 1100 Between 90° and 135° ECAE Processes

A. Hasani* and S. Feyzi

Mechanical Engineering Group, Faculty of Engineering, University of Kurdistan, PB 416, PC 66177-15175, Sanandaj, Kurdistan Province, Iran

ARTICLE INFO

Article history:

Received 12 February 2023
Reviewed 18 March 2023
Revised 14 April 2023
Accepted 16 April 2023

Keywords:

Anisotropy
ECAE
Nano-indentation test
Texture evolution
Aluminum 1100

Please cite this article as:

A. Hasani, S. Feyzi, Comparison of plastic anisotropy and crystallographic texture evolution of aluminum 1100 between 90° and 135° ECAE processes, *Iranian Journal of Materials Forming*, 10(1) (2023) 26-38.

ABSTRACT

A rolled sheet of aluminum 1100 was processed by two ECAE dies with inner corner angles of 90° and 135°. The samples were processed using route A up to 4 and 10 passes in ECAE 90° and 135°, respectively. The mechanical behaviors of initial and processed materials were evaluated by nano-indentation and compression tests carried out at three different orthogonal directions, at room temperature. Crystallographic texture evolution during two different ECAE processes has been also studied. A considerable reduction in mechanical anisotropy is displayed for processed materials compared to the initial material by nano-indentation tests. Though there is appreciable progress in mechanical isotropy for processed materials by 135° ECAE, compared to the 90° case. Studying crystallographic texture evolutions reveals that ECAE 135° is more capable than ECAE 90° in the development of cube components; however, the rate of texture evolution is slower in ECAE 135°. Dissimilar prominent texture components are also developed by two different ECAE processes.

1. Introduction

Ultra-fine grain (UFG) or nanostructured materials could be achieved by imposing severe plastic deformation processes (SPD) on a polycrystalline metal sample, due to the reduction in the grain size [1]. Equal channel angular extrusion (ECAE) has been allocated the most attention among available different SPD methods [2] in which extremely high strains can be introduced into metallic materials by repetitive passes through a special die without any variation in the cross-section of the samples [1-4]. The most frequent application of ECAE is not only due to the possibility producing of billets (even in relatively large sizes [5]) without any porosity or contaminants, but also its potential to introduce developed materials that can be used in different applications [6, 7]. ECAE could present unusual but desirable mechanical properties for

* Corresponding author
E-mail address: a.hasani@uok.ac.ir (A. Hasani)
https://doi.org/10.22099/IJMF.2023.46818.1248

processed metals (e.g., high strength and low temperature super plasticity [1]). Equality in the cross-section allows the reinsertion of the samples repeatedly, which imposes a strain-path change, inevitably. The sequence and the nature of the strain path could be modified using different optional rotations of the sample about its long axis between the passes, known as ECAE routes. Furthermore, a wide range of plastic strain could be imposed in this process depending on the ECAE die angle. However, the unavoidable limitation in this process is the exhibition of anisotropy in the mechanical properties of the extruded samples, which may be dependent on the difference in the straining and pressing directions [8]. The importance of this mechanical anisotropy could be revealed by its influences on the subsequent shaping operations.

The anisotropy in ECAE has been already evaluated experimentally [8-14]; however, except for Ref. [9] which studied anisotropy in ECAE 135°, other works have concentrated on the most common ECAE die angle of 90°. Compression tests, in addition to studying crystallographic texture evolutions, have been frequently used to investigate the occurrence procedure of plastic anisotropy in ECAE [9-12]. The micro-hardness test has also been performed in addition to the compression test to study mechanical anisotropy in ECAE samples [8, 13-15].

The mechanical properties of aluminum 1100 have been measured recently using the nano-indentation test [16]. Even though this test has not been already used for ECAE, however considering the nanoscale grain size of its products, the nano-Indentation test could be employed as the preferred method for studying anisotropy in ECAE compared to the micro-hardness test. Nano- and micro-hardness tests are compared in reference [17] and the reason for the preference of nano-hardness test is explained. The main point in the hardness test is the indentation size effect; therefore, due to lower indentation size effect, the nano-indentation test has a higher measurement accuracy than the micro-hardness test, and therefore provides more accurate data. Undoubtedly, this accuracy is more important in the materials with nanoscale grain size, and therefore an appropriate test should be used, especially in accordance with its structural size. On the other hand, any comparison has not been performed previously between the two different ECAE processes; furthermore, the texture evolution has not been studied seriously in ECAE 135°. Hence, in the present work, mechanical anisotropy evaluation of aluminum 1100 in two dissimilar ECAE die angles 90° and 135° have been compared. A comparison has been done between the samples with nearly the same equivalent plastic strain imposed by two different ECAE processes. Mechanical properties have been measured using compression, and nano-indentation tests were performed in different directions of the ECAE samples at room temperature. It should be noticed that the compression test and the nano-indentation experiments are two entirely different testing methods. In contrast, in the nano-indentation experiment where only some selected points and localized regions around them are comprised, the whole bulk of the specimen affects the test results in the compression test. The crystallographic texture evolution during two ECAE processes is also studied and analyzed. It is revealed that despite the relatively similar equivalent plastic strain, the anisotropy evolution in two different ECAE processes could be completely different.

2. Experimental Procedure

2.1. ECAE tests

A rolled sheet of aluminum 1100 with 10 mm thickness is used in this study. In order to preserve the anisotropy and mechanical properties resulting from the rolling process, no heat treatment has been done on the initial samples. Prismatic ECAE samples with 10×10 mm^2 cross-section and 70 mm length were prepared along the rolling direction of the rolled sheet. The sampling location is shown in Fig. 1.

The ECAE die geometry, as the main factor in the present work, is introduced in Fig. 2. In this figure d is channel size, and Φ and Ψ are the die inner corner angle and outer corner angle, respectively.

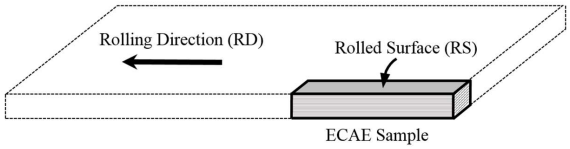

Fig. 1. Location of ECAE sample in the as-received rolled sheet material.

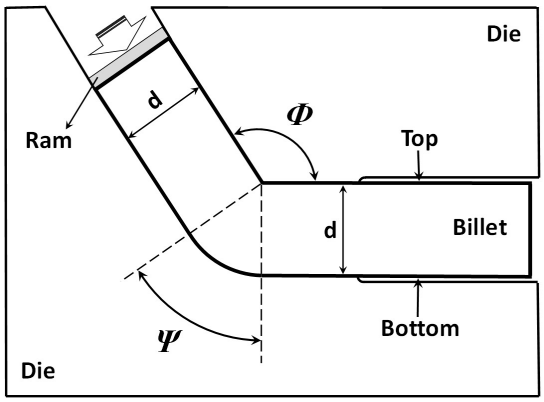

Fig. 2. ECAE die geometry including the die angle Φ, and the corner angle Ψ.

Two ECAE dies with inner corner angles of 90° and 135°, without any outer corner angles (Ψ=0°) have been fabricated from heat treated 4340 steel. The dies have square cross section 10×10 mm^2 in inlet and outlet channels (Fig. 3).

In both cases, the first ECAE pass was performed somehow the rolled surfaces of the samples were faced towards the side walls of the channels. Fig. 4 shows the situation of the ECAE samples in the inlet channel of the dies at the first step of the ECAE test.

The accumulated shear strain in an ECAE die is given by the following equation [2]:

$$\gamma = \left[2\cot\left(\frac{\Phi}{2}+\frac{\Psi}{2}\right)+\Psi\mathrm{cosec}\left(\frac{\Phi}{2}+\frac{\Psi}{2}\right)\right] \qquad (1)$$

where, Φ and Ψ are the die and outer corner angles, respectively (see Fig. 2). Subsequently, using Eq. (1), the von-Mises equivalent strain in ECAE could be found as:

$$\varepsilon_{eq} = \frac{\gamma}{\sqrt{3}} = \frac{1}{\sqrt{3}}\left[2\cot\left(\frac{\Phi}{2}+\frac{\Psi}{2}\right)+\Psi\mathrm{cosec}\left(\frac{\Phi}{2}+\frac{\Psi}{2}\right)\right] \qquad (2)$$

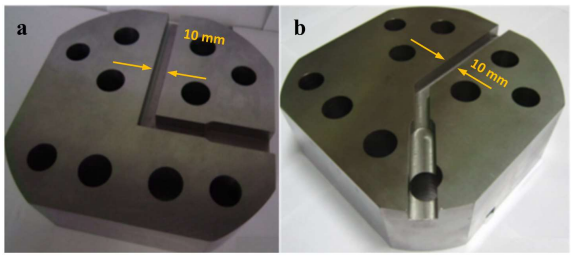

Fig. 3. Two ECAE dies used in the present work, (a) 90° and (b) 135°.

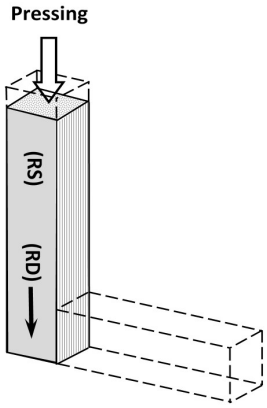

Fig. 4. Position of the initial sample in the inlet channel of the ECAE die at the first step.

Considering the sharp outer corner (Ψ=0°), the theoretically executed plastic strain of ECAE 135° is less than half of the ECAE 90°, in each pass. Thus, an appropriate number of passes should be chosen in ECAE 135° concerning ECAE 90° to achieve approximately the same accumulated strain on the experimented samples. The material was treated using route A by 4 and 10 passes in 90° and 135° ECAE dies, respectively. These number of passes have been considered because a nearly theoretical accumulated strain of 4.62 and 4.78 could be obtained in the samples of 90° and 135° ECAE dies, respectively. The ECAE tests have been performed at room temperature with a punch speed of ~0.1 mm/s. To reduce friction between the samples and the channel walls, molybdenum disulfide (MoS_2) was used as a lubricant.

2.2. Compression tests

After ECAE tests, cylindrical parallelepipeds compression test samples were machined from the

central part of the extruded billets with 5 mm diameter and 8 mm heights where the central axis of the samples aligned to three orthogonal directions X, Y, and Z illustrated in Fig. 5; so, the machined samples are named the X, Y, and Z samples.

These sample dimensions were selected to give an aspect ratio of height/width equal to 1.6. It should be noticed in compression tests that high aspect ratios lead the samples to buckle while in very low aspect ratios the surfaces of the samples have a bearing on the loading platens [3]. All of the compression tests were carried out at room temperature using a head speed of 0.3 mm/min. Similar tests were also performed via initial samples prepared from the as-received billets for comparison purposes. To stay away from any interference of the machining on the results, each test was repeated three times.

2.3. Nano-indentation tests

Nano-indentation test samples were also prepared in the form of small tetragonal specimens with 4 mm thick and a 10×10 mm^2 cross section area from the central parts of the extruded samples; where the normal axis of the cross section is parallelized to the orthogonal X, Y, and Z directions, as shown in Fig. 6.

Considering the significant influence of the surface finish on the nano-indentation test results, the surface of the samples was ground with abrasive papers 180-2500 and polished using 1 µm alumina suspension to achieve mirror-like surfaces.

The nano-indentation tests were carried out using a triboscope system (Hysitron Inc., USA) with a cube corner indenter. The ISO 14577 standard [18] has been used for calibration of the testing instrument. It has already been shown [19, 20] that the penetration depth of indenter affects the measured mechanical properties of materials. Based on this standard, the indentation depth should be sufficiently deep to minimize the surface effect; however, in most cases after a depth of 200 nm the measured properties are almost stable. An indentation load of about 260 µN was applied in the present study for which different maximum indentation depths were achieved for different cases. It should be noticed that several indentations were performed on the randomly selected locations on the surface of the samples which lead to taking at least five nearly load-displacement curves from the tests. Meanwhile, the

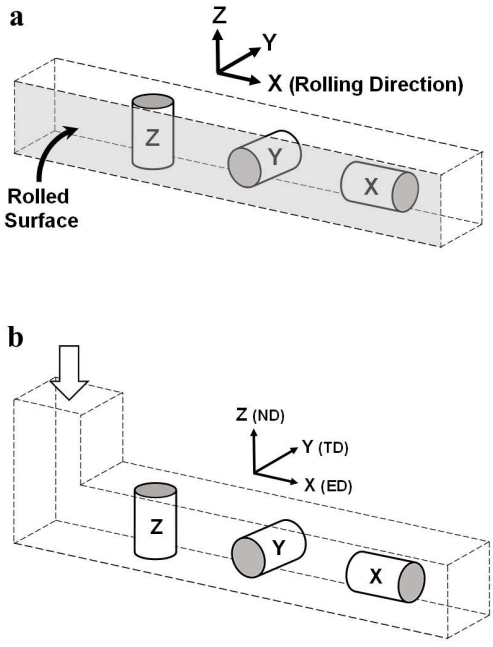

Fig. 5. Orientation of compression test samples with respect to the billets: (a) initial and (b) processed samples.

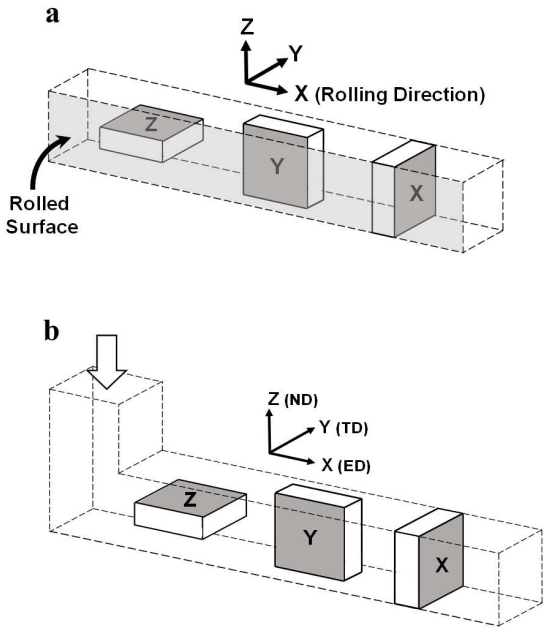

Fig. 6. Orientation of nano-indentation test samples with respect to the billets, (a) initial and (b) processed samples.

surface roughness quality of the tested samples was surveyed at the indentation areas using atomic force microscopy (AFM). The AFM images were also utilized for surface investigations, before and after the experiments (Fig. 7).

Mechanical properties of the nano-indentation test samples could be calculated using Oliver–Pharr's method [21] and relations derived from the theory of contact mechanics.

2.4. Crystallographic texture

To have a more complete comparison between the abilities of ECAE 90° and 135°, the texture evolution during these processes is studied. The crystallographic textures before and after pressing were measured at the University of Lorrain (Metz, FRANCE). It is noteworthy that just route A is considered in ECAE tests. The number of passes has been considered as 5 and 10 for 90° and 135° ECAE, respectively. To compare the results with the previous work [22], one more pass is carried out for the 90° case in this section. Texture measurements were carried out from the mid-horizontal plane of the sample (XY plane of Z sample in Fig. 6).

Since the orientation distribution functions (ODFs) describe textures better than pole figures, this study is carried out using the ODF method for texture analysis of materials processed just through route A of both ECAE processes that also share identical starting materials. As the sections φ_2= 0° and φ_2= 45° of the ODF space contain the most important orientations, they are usually used to present ODFs of shear textures for FCC materials. Accordingly, these sections will be employed in the present work. Note that the ODFs were calculated without imposing any sample symmetry and so the range of the φ_1 Euler angle is from 0° to 360°.

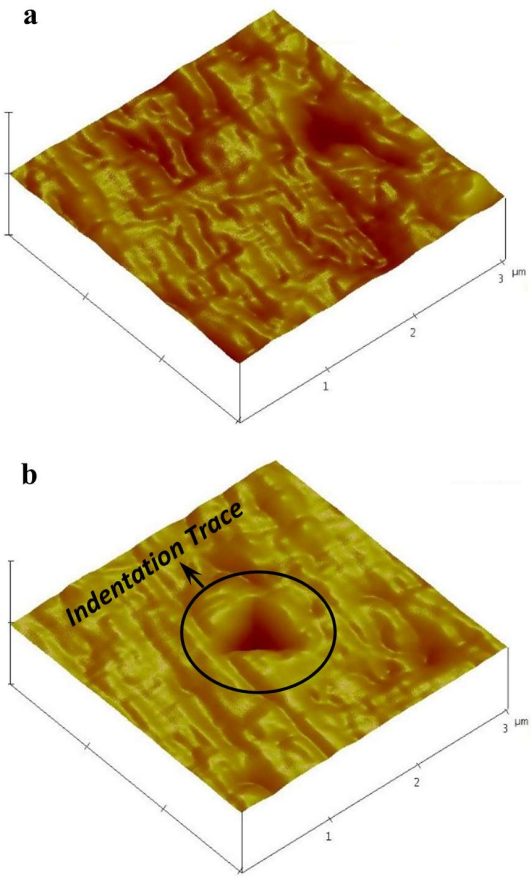

Fig. 7. AFM images of aluminum 1100 surface, (a) before and (b) after the nano-indentation test.

3. Results and Discussion

3.1. Compression test

The stress (σ) versus strain (ε) curves obtained from compression tests at three different directions for specimens processed in two different ECAE die angles of 90° and 135° are offered in Fig. 8. The curves of the initial (as-received) material are also presented for comparison.

The materials were processed through 4P and 10P in 90° and 135° ECAE die angles, respectively, where P denotes the number of ECAE passes in Fig. 8.

One can see that the processed materials in both ECAE die angles, present higher flow stress, in all directions, compared with the as-received material. The processed materials were also found in the same region of detected maximum stress. The as-received material presents different yield and flow stresses, depending on the compression direction. Though these differences are decreased in the 90° ECAE case; they were, however, significantly minimized in the 135° ECAE die. As can be seen, a meaningful harmony is presented in ECAE 135° which can be interpreted as the less mechanical

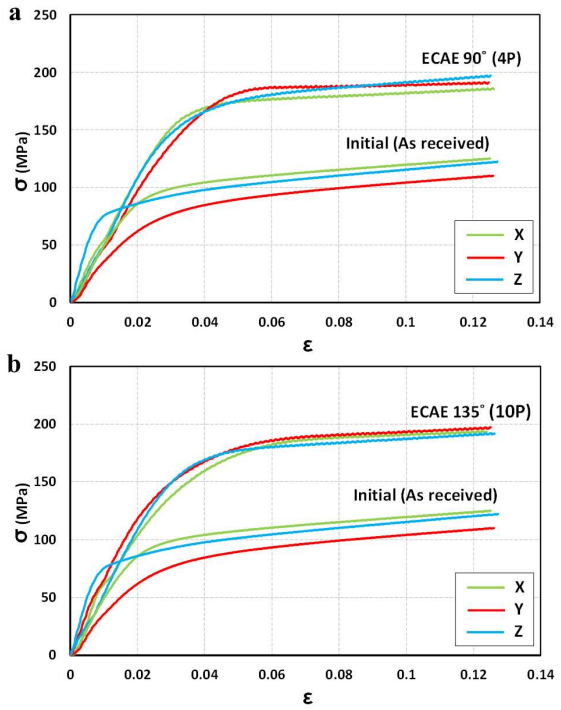

Fig. 8. Stress strain curves of Al-1100 at different directions for initial (as received) and processed specimens at (a) 90°, and (b) 135° ECAE die angles.

anisotropy for processed materials by 135° ECAE, compared to the 90° case. To clarify the difference in the hardening behavior of the initial and processed materials at different X, Y, and Z directions, other comparisons among the respected stress-strain curves are offered in Fig. 9.

At X and Y directions, the stress-strain curve in the ECAE 135° shows a very gradual yielding; whereas the samples processed through ECAE 90° present a more restricted yielding area. After yielding, the 90° case displays lower flow stress. A good agreement between curves of the two different ECAE cases could be seen in Z direction; though a faintly higher flow stress is displayed for ECAE 90°, unlike the other directions.

Regardless of the yielding part, all of the curves present an approximately linear segment which means that the initial and processed materials are strain hardened at an almost constant rate. Subsequently, the slope of the curves at this part has been considered as the sign of the hardening rate, $\theta = \Delta\sigma/\Delta\varepsilon$. The measured slopes are noted in Fig. 9 and presented in Table 1.

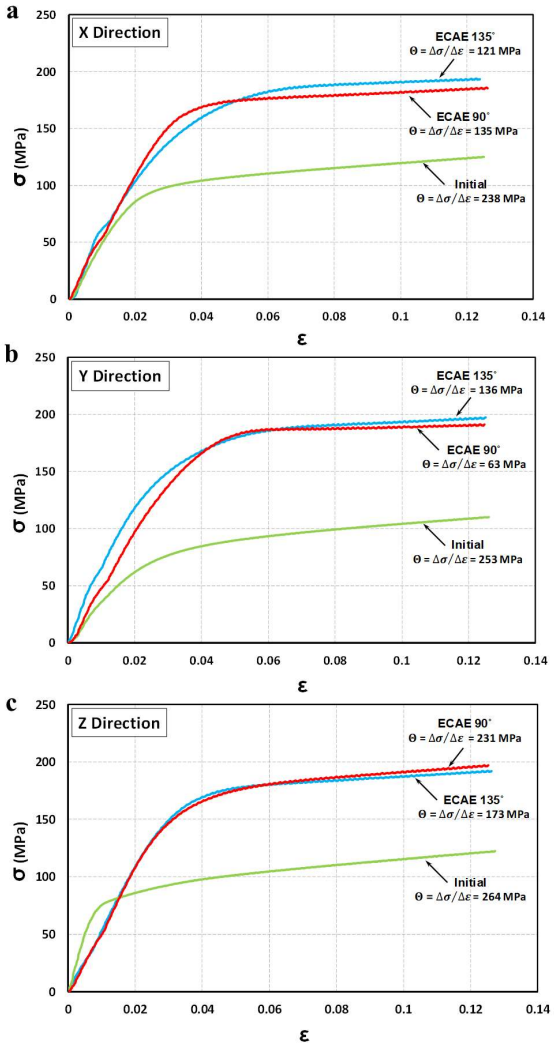

Fig. 9. Comparison of stress-strain curves of initial and processed samples in (a) X, (b) Y, and (c) Z.

Table 1. Strain hardening rate of the initial and processed materials in different directions

	X Direction	Y Direction	Z Direction
	$\theta = \Delta\sigma/\Delta\varepsilon$ MPa	$\theta = \Delta\sigma/\Delta\varepsilon$ MPa	$\theta = \Delta\sigma/\Delta\varepsilon$ MPa
Initial	238	253	264
ECAE 90°	135	63	231
ECAE 135°	121	136	173

For more clarification in the strain hardening rate variations, the measured slopes, presented in Table 1, are analyzed in Fig. 10.

Despite the dissimilarities in stress-strain curves presented in Fig. 9 for initial material in different directions, Fig. 10(a) reveals that there is not a large anisotropy in strain hardening rate for the initial material. It is also illustrated that, although this anisotropy is not increased significantly by the ECAE 135° process, it is, however, considerably improved in ECAE 90° material.

It is observed in Fig. 10(b) that the material processed by ECAE exhibits a lower hardening rate in each direction, compared to the initial material. This reduction in strain hardening is also found in X and, especially, in Y directions. In the Y direction, contrary to the X and Z directions, the rate of hardening in ECAE 90° is subordinated concerning ECAE 135°.

3.2. Nano indentation test

The load-displacement curves for initial and processed materials in different directions have been obtained from nano-indentation tests. Fig. 11 shows a load-displacement curve in respect to the initial sample in X direction.

According to the test results, Young's modulus and nano-hardness of the samples were found and presented in Table 2. The results of Table 2 are also compared in Figs. 12 and 13.

Figs. 12(a) and 13(a) show an obvious mechanical anisotropy in the initial material, where a difference of about 14% and 28% could be found between different directions for Young's modulus and nano-hardness, respectively. However, it is observed that these dissimilarities are about 5% and 9% for ECAE 90°; while 3% and 10% have been measured for ECAE 135°. Therefore, a considerable reduction in the mechanical property's variations have been revealed in processed

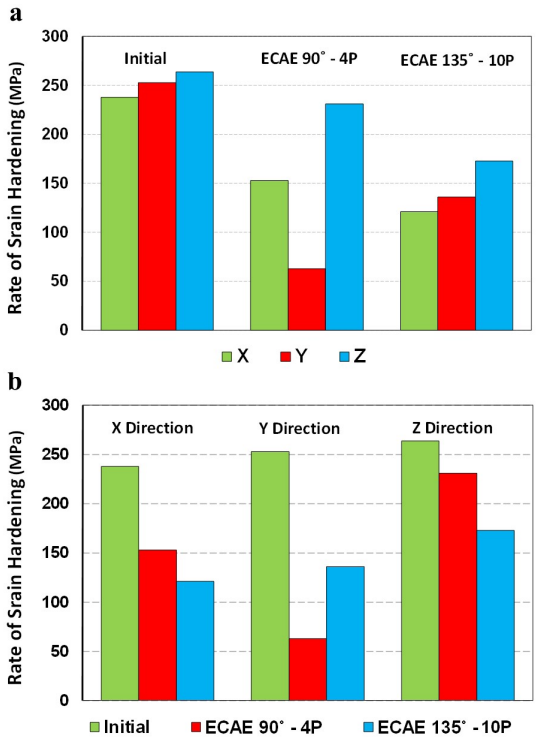

Fig. 10. Comparison of strain hardening rate of initial and processed materials in different directions.

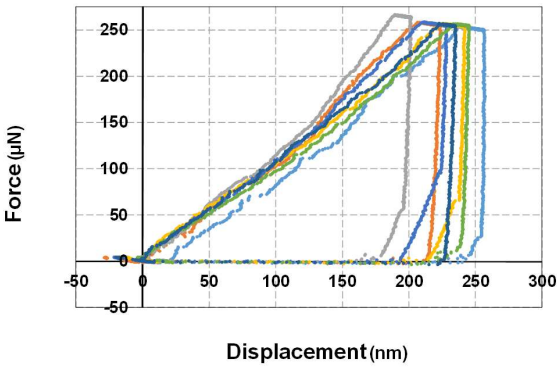

Fig. 11. Load-displacement curve of the initial sample in X direction.

Table 2. Young's modulus and nano-hardness of the initial and processed materials in different directions.

	X Direction		Y Direction		Z Direction	
	Young's modulus (GPa)	Nano-hardness (GPa)	Young's modulus (GPa)	Nano-hardness (GPa)	Young's modulus (GPa)	Nano-hardness (GPa)
Initial	74.55	0.755	83.29	0.81	71.75	1.045
ECAE 90°	83.01	1.052	83.67	0.95	79.48	0.99
ECAE 135°	81.49	1.097	79.48	1.123	79.15	1.01

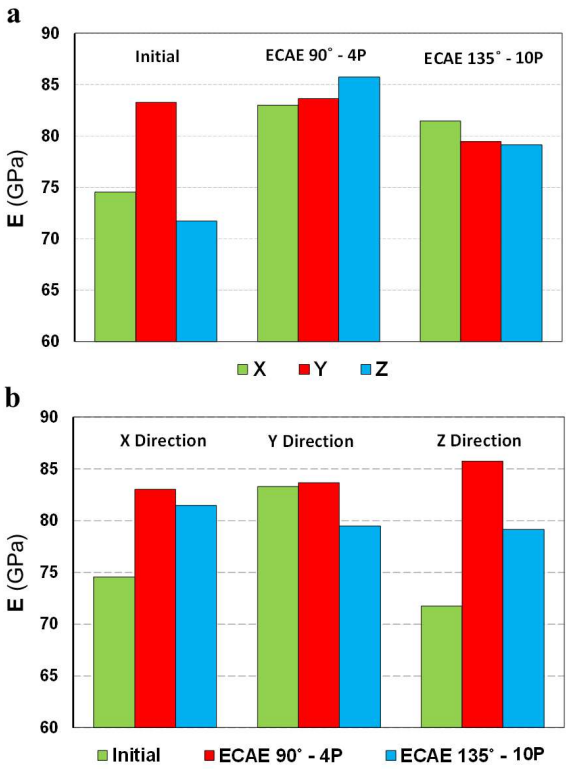

Fig. 12. Comparison of Young's modulus of the initial and processed materials in different directions.

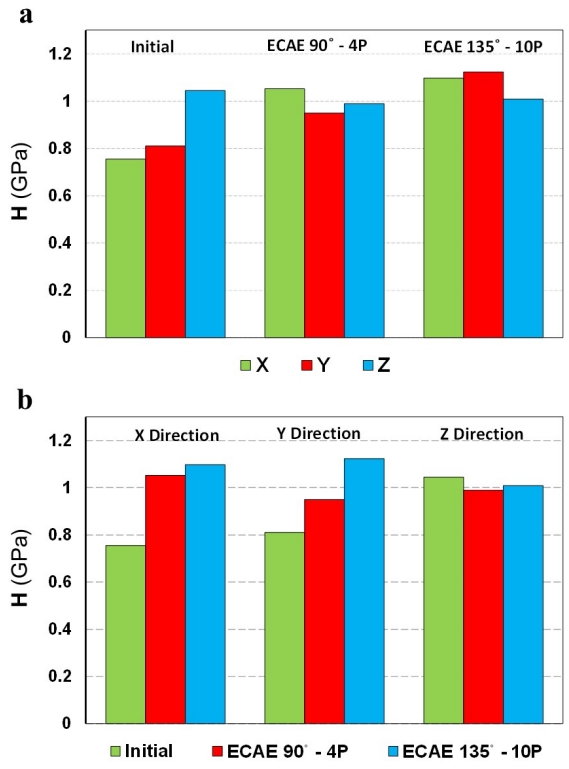

Fig. 13. Comparison of nano-hardness of the initial and processed materials in different directions.

materials, compared to the initial material; though, there are no appreciable differences between processed materials, in two different ECAE die angles.

Fig. 12(b) shows that Young's modulus of pressed materials in X direction has increased compared to the as-received material, though Young's modulus in ECAE 90° is just higher than ECAE 135°. Young's modulus of initial material in the Y direction has not increased fairly in ECAE 90° but decreased considerably in ECAE 135°. In the Z direction, processed materials show an extensive augmentation in Young's modulus, though ECAE 135° presents a noticeably lower Young's modulus compared to the 90° case.

It is revealed that ECAE 90° monopolized the maximum Young's modulus, and ECAE 135° shows lower Young's modulus than 90° in each direction. The nano-hardness of as-received material has increased using both ECAE processes in X and Y directions, as shown in Fig. 13(b). Although hardness of the sample of ECAE 135° is not much higher than ECAE 90° in the X direction, but a considerable increase in hardness could be seen in ECAE 135° concerning ECAE 90°, in the Y direction. Nano-hardness of the extruded samples has decreased, compared to the initial sample in the Z direction; where inconsiderable variance in nano-hardness between the two ECAE processes is presented.

3.3. Crystallographic texture evolution

The texture of the starting material is shown in Fig. 14 in the 0° and 45° sections of the ODF which indicates the presence of a very strong cube texture in the material. ATEX software [23] was used to plot the crystallographic textures.

The measured ODF for all the 90° ECAE deformed samples along with a key figure of respected ideal orientations are shown in Fig. 15.

As the deformation mechanism in ECAE is near simple shear in the intersection plane of the inlet and exit channels, the same ideal texture components, previously known for simple shear, could be considered for ECAE process just with a rotation of 45° with respect to the ECAE reference system for 90° ECAE [24]. The same

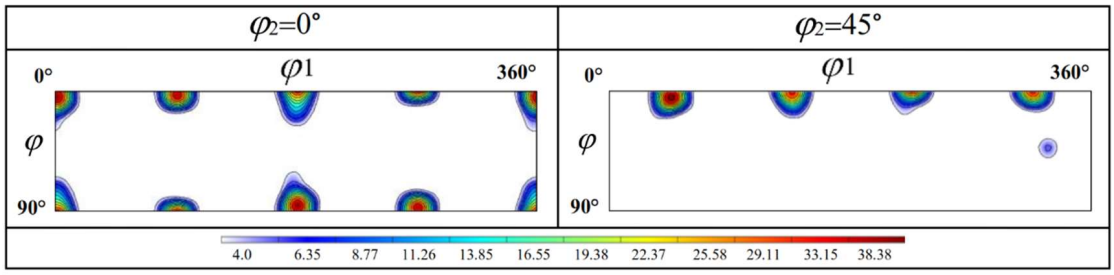

Fig. 14. Starting texture in φ_2= 0° and φ_2= 45° sections of the ODF.

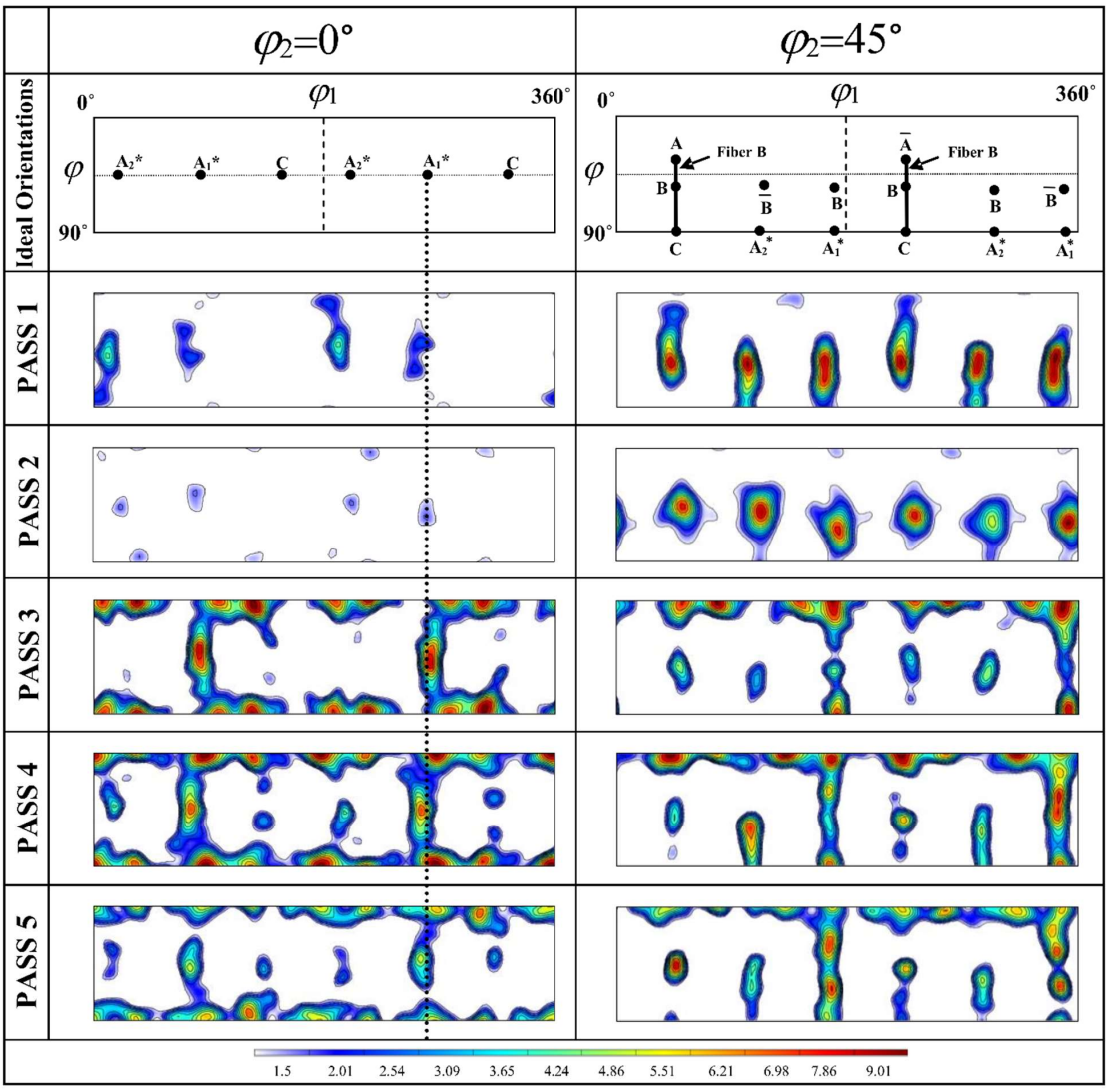

Fig. 15. Measured ODFs with ideal orientations for all the 90° ECAE deformed samples in φ_2= 0° and φ_2= 45° sections.

procedure has been considered in order to find the ideal texture components for 135° ECAE; but with a rotation of 67.5°.

Fig. 16 shows the ideal orientation with measured textures in φ_2=0° and φ_2=45° sections of the ODF for 135° the ECAE process. Note that to shorten the ODF figures, just the even ECAE passes in addition to the first pass are presented in Fig. 16.

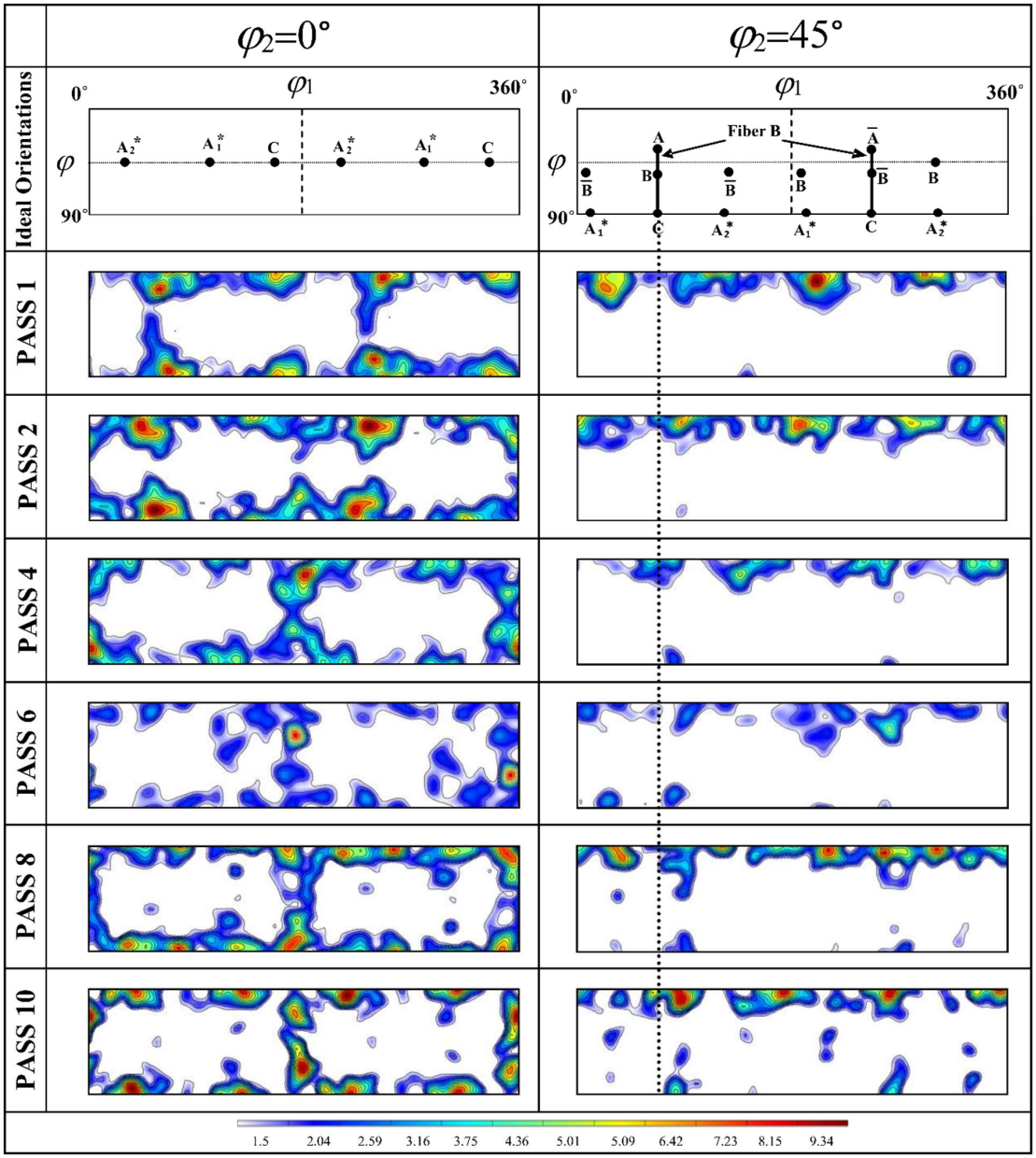

Fig. 16. Ideal orientation key and measured ODFs for the 135° ECAE deformed samples in φ_2= 0° and φ_2= 45° sections.

One can see in Fig. 15 that a very systematic texture evolution in the ODF plots is presented by the 90° ECAE processed material. Appreciable changes occur in the texture, even after one pass takes place; and the initially very strong cube texture components disappears as well. The textures of processed sample gradually weakened after the second pass. In pass 3 the remnants of the cube related texture components are strengthened considerably and distributed as the fibers called cube-fibers [22]. The intensities of components along these fibers are decreased by the deformation process; however, they still prevail at the final pass. It is obvious that A_1^* is the prominent component in the texture; while A_2^* and C components are vanishingly weak, for all the passes. The A, $\bar{A}$ and B, $\bar{B}$ components are not seen after the first pass but developed progressively by increasing the pass number.

Considering the position of A_1^* as the perdurable

component of the texture and comparing it to the ideal orientation (see the dot line in Fig. 15), the texture could not reach its ideal position at the first pass; however, it did so at the second pass. One can see a little deviation by increasing the φ_1 in pass 3; however, pass 4 presents a noticeable decreasing in the φ_1; while it remains approximately constant at the final pass. Concerning the 135° ECAE, Fig. 16 illustrates that the changes in the texture are absolutely apparent after the ECAE deformation. It should be noticed that the texture evolution in 135° ECAE is slower than 90° ECAE due to the lower plastic shear in one pass of 135° ECAE (0.828 for simple shear) compared to the 90° ECAE (which is a shear of 2.0). The initially very strong cube texture components have not only disappeared but also developed and prevailed from the first to the final pass. At the first pass, the cube components tend to produce cube fibers by appearance the weak A_2^* component, pending the slight rotation of the texture towards the ideal orientation. After the first pass, a relatively weak texture develops and slightly weakens up to the sixth pass; and strengthens subsequently up to the final pass.

In spite of the A_1^* and A_2^* components which are vanishingly weak during the deformation, Fig. 16 indicates that the C component has appeared from the second pass and remains as the prominent component in the texture. There is a noticeable and approximately fixed deviation for this component from its ideal position, in all the passes (notice the dot line in Fig. 16). The B and $\bar{B}$ components are seen just in the final pass, while the A and $\bar{A}$ have never been developed.

4. Conclusion

Prismatic samples prepared from a rolled sheet of aluminum 1100 were processed at room temperature by ECAE in two different die angles of 90° and 135°. The samples were processed up to 4 and 10 passes by ECAE 90° and 135° respectively; where an approximately same equivalent plastic strain could be imposed on the samples by these two different ECAE processes.

Hence, the compression and nano-indentation tests were conducted at room temperature using samples cut in different orientations concerning the pressing direction. All of the measurements were taken on three orthogonal planes before and after being processed by ECAE.

The crystallographic texture of the initial and processed materials just in route A were measured using X-ray diffraction. Texture measurements are carried out for all passes of ECAE 90°, however, just the even ECAE passes in addition to the first pass are measured in ECAE 135°. For the 90° case, the fifth pass was also carried out, just to compare the results of texture evolution with the previous work. The ODF method with φ_2= 0° and φ_2= 45° sections of the ODF space are used for texture analysis.

The following conclusions were gained:

1. The same range of measured maximum stress but higher than as-received material is offered for two different ECAEs processed. Furthermore, dissimilarities in the stress-strain curves of the initial material, depending on the compression test direction, are considerably reduced in the 90° ECAE case, but significantly diminished in the 135° ECAE die. An expressive harmony in stress-strain curves in ECAE 135° indicated less mechanical anisotropy for processed materials by 135° ECAE, compared to the 90° case.
2. A considerable reduction in mechanical anisotropy for processed materials concerning the initial material is revealed by the nano-indentation test. However, there is no appreciable difference between the two unlike ECAE-processed materials, in this respect.
3. Although the texture evolution in ECAE 135° is slower than ECAE 90°, ECAE 135° is more capable to develop cube components. In both ECAE processes, a non-even intensity cube fiber is formed by the rotated cube components. There is no similar prominent component in the textures developed by two different ECAE processes; A_1^* and C components are presented in this regard by ECAE 90° and 135°, respectively. A little deviation between the developed texture and respected ideal orientation is detected in both deformation processes.

Acknowledgments

The authors are thankful to Mr. J.J. Fundenberger for his collaboration in crystallographic texture measurements.

Conflict of Interests

The authors declare that they have no known competing financial interests or personal relationships that could have appeared to influence the work reported in this paper.

Funding

This research has not received any funds.

5. References

[1] R.Z. Valiev, T.G. Langdon, Principles of equal-channel angular pressing as a processing tool for grain refinement, *Progress in Materials Science*, 51(7) (2006) 881-981.

[2] R.Z. Valiev, Y. Estrin, Z. Horita, T.G. Langdon, M.J. Zechetbauer, Y.T. Zhu, Producing bulk ultrafine-grained materials by severe plastic deformation, *JOM*, 58 (2006) 33-39.

[3] V.M. Segal, Equal channel angular extrusion: from macromechanics to structure formation, *Materials Science and Engineering: A*, 271(1-2) (1999) 322-333.

[4] I.J. Beyerlein, L.S. Tóth, Texture evolution in equal-channel angular extrusion, *Progress in Materials Science*, 54(4) (2009) 427-510.

[5] Z. Horita, T. Fujinami, T.G. Langdon, The potential for scaling ECAP: effect of sample size on grain refinement and mechanical properties, *Materials Science and Engineering: A*, 318(1-2) (2001) 34-41.

[6] Y.T. Zhu, T.C. Lowe, T.G. Langdon, Performance and applications of nanostructured materials produced by severe plastic deformation, *Scripta Materialia*, 51(8) (2004) 825-830.

[7] R.Z. Valiev, M.J. Zehetbauer, Y. Estrin, H.W. Höppel, Y. Ivanisenko, H. Hahn, G. Wilde, H.J. Roven, X. Sauvage, T.G. Langdon, The innovation potential of bulk nanostructured materials, *Advanced Engineering Materials*, 9(7) (2007) 527-533.

[8] C. Xu, Z. Száraz, Z. Trojanová, P. Lukáč, T.G. Langdon, Evaluating plastic anisotropy in two aluminum alloys processed by equal-channel angular pressing, *Materials Science and Engineering: A*, 497(1-2) (2008) 206-211.

[9] F.S.J. Poggiali, C.L.P. Silva, P.H.R. Pereira, R.B. Figueiredo, P.R. Cetlin, Determination of mechanical anisotropy of magnesium processed by ECAP. *Journal of Materials Research and Technology*, 3(4) (2014) 331-337.

[10] I.J. Beyerlein, S. Li, and D.J. Alexander, Modeling the plastic anisotropy in pure copper after one pass of ECAE, *Materials Science and Engineering: A*, 410 (2005) 201-206.

[11] I.J. Beyerlein, D.J. Alexander, C.N. Tomé, Plastic anisotropy in aluminum and copper pre-strained by equal channel angular extrusion, *Journal of Materials Science*, 42 (2007) 1733-1750.

[12] I.J. Beyerlein, C.N. Tomé, Modeling transients in the mechanical response of copper due to strain path changes, *International Journal of Plasticity*, 23(4) (2007) 640-664.

[13] M. Prell, C. Xu, T.G. Langdon, The evolution of homogeneity on longitudinal sections during processing by ECAP, *Materials Science and Engineering: A*, 480(1-2) (2008) 449-455.

[14] C. Xu, M. Furukawa, Z. Horita, T.G. Langdon, The evolution of homogeneity and grain refinement during equal-channel angular pressing: A model for grain refinement in ECAP, *Materials Science and Engineering: A*, 398(1-2) (2005) 66-76.

[15] C. Xu, T.G. Langdon, The development of hardness homogeneity in aluminum and an aluminum alloy processed by ECAP, *Journal of Materials Science*, 42 (2007) 1542-1550.

[16] A. Karimzadeh, M.R. Ayatollahi, M. Alizadeh, Finite element simulation of nano-indentation experiment on aluminum 1100, *Computational Materials Science*, 81 (2014) 595-600.

[17] L. Qian, M. Li, Z. Zhou, H. Yang, X. Shi, Comparison of nano-indentation hardness to microhardness, *Surface and Coatings Technology*, 195(2-3) (2005) 264-271.

[18] ISO 14577, in Part 2: Verification and Calibration of Testing Machines, Part 3: Calibration of Reference Blocks, Geneva, Switzerland, 2002.

[19] Y. Hu, L. Shen, H. Yang, M. Wang, T. Liu, T. Liang, J. Zhang, Nanoindentation studies on nylon 11/clay nanocomposites, *Polymer Testing*, 25(4) (2006) 492-497.

[20] T. Liu, I.Y. Phang, L. Shen, S.Y. Chow, W.D. Zhang, Morphology and mechanical properties of multiwalled carbon nanotubes reinforced nylon-6 Composites, *Macromolecules*, 37(19) (2004) 7214-7222.

[21] A.C. Fischer-Cripps, Nanoindentation, Springer, New York, 2011, pp. 181-198.

[22] S. Suwas, R.A. Massion, L.S. Tóth, J.J. Fundenberger, B. Beausir, Evolution of texture during equal channel angular extrusion of commercially pure aluminum: experiments and simulations, *Materials Science and Engineering: A*, 520(1-2) (2009) 134-146.

[23] B. Beausir, J.J. Fundenberger, Analysis tools for electron and X-ray diffraction, ATEX–software, Université de Lorraine, Metz, France, 2017.

[24] L.S. Tóth, R.A. Massion, L. Germain, S.C. Baik, S. Suwas, Analysis of texture evolution in equal channel angular extrusion of copper using a new flow field, *Acta Materialia*, 52(7) (2004) 1885-1898.